Journal of Modern Researches on Electronic Defense Systems

Receive: 9 February 2025 Accept: 18 April 2025

Enhanced Performance of a Terahertz Rectangular Resonator Filter Utilizing Graphene-Integrated Dual Slit Configuration

Abolfazl Vaghayei[1], Majid Afsahi*[2], Mohammad Danaie[3]
Corresponding Author: m_afsahi@semnan.ac.ir

[1] PhD Candidate, Electrical & Computer Engineering Faculty, Semnan University, Iran.
[2] Associate Professor, Electrical & Computer Engineering Faculty, Semnan University, Iran.
[3] Associate Professor, Electrical & Computer Engineering Faculty, Semnan University, Iran.

Abstract – *This scientific article presents an innovative plasmonic filtering device featuring a distinctive geometric configuration, characterized by the rectangular ring resonator made from graphene, which includes two narrow gaps. This unique design facilitates dynamic control over the working frequency range and the transmission peak frequency. By carefully adjusting the width of the graphene nanoribbons and manipulating the coupling distance between the waveguide and the resonator, the device allows for precise modifications of its operational characteristics. The filter is designed to operate in a single-mode capacity, showcasing exceptional frequency response performance. Furthermore, one of its noteworthy attributes is its sensitivity to variations in surrounding mediums, positioning it as a promising candidate for advanced biosensor applications that require high responsiveness. This novel structure not only contributes to the miniaturization of plasmonic filtering devices but also holds the potential for seamless integration into compact plasmonic circuitry. In summary, when compared to various other structures, the proposed design stands out due to its minimized dimensions, single-mode functionality, and superior frequency response capabilities, making it a significant advancement in the field.*

Keywords: *Plasmonic filtering device, ring resonator, graphene, dual narrow gap, graphene nanoribbons width, junction spacing, single mod.*

1. Introduction

In recent decades, there has been considerable progress in the field of optics and terahertz frequencies, presenting promising alternatives to microwave technologies [1]. Terahertz technologies offer the advantages of a flexible and wide bandwidth range, material penetration capabilities, and support for device miniaturization [2]. This progress has led to extensive research on terahertz devices for diverse applications such as security, biomedicine, medical spectroscopy, astronomy, molecular detection, and inter-satellite communications [3,4]. Furthermore, the unique properties of materials like graphene have significantly enhanced the development of terahertz technologies. For instance, graphene's exceptional electrical conductivity and high thermal stability open new avenues for creating highly sensitive terahertz sensors and antennas, which can be utilized in environmental monitoring and hazardous material detection [5]. Moreover, integrating graphene with terahertz devices has potential applications in high-speed wireless communication systems, enabling faster data transfer rates and improved signal quality [6]. Additionally, research is exploring the use of terahertz radiation in non-invasive imaging techniques, which could revolutionize fields like pharmaceuticals and food safety by allowing for the detection of counterfeit products and contamination without damaging the samples [7-9]. Overall, the synergy between terahertz technology and graphene not only broadens the scope of applications but also paves the way for innovative solutions in various disciplines, including telecommunications, healthcare, and nanotechnology [10-12]. At terahertz frequencies, conventional metals face technical challenges at the nano-atomic level. As a result, noble metals are required to support the propagation of surface plasmons [13]. Surface plasmons are free electron oscillations occurring at the metal-dielectric interface [14,15]. Surface plasmon polaritons (SPP) are particularly useful in integrated optical circuits due to their ability to

manipulate electromagnetic waves at the nanoscale [16,17]. Graphene, with its nano-thin atomic structure, has emerged as an exceptional material in this context [18]. The hexagonal arrangement of carbon atoms in graphene forms sp2-bonded lattice structures, offering unique thermal, optical, and electrical properties [19]. Graphene's negative permittivity in the terahertz regime enables the propagation of surface plasmons with low losses. Moreover, by adjusting the applied voltage to the graphene layer, the material's permittivity can be altered, providing control over its conductivity through bias voltage. In addition to supporting surface plasmon propagation, graphene's excellent thermal, optical, and electrical properties make it an outstanding choice for designing devices in the terahertz frequency band [20-23]. Given the rapid advancements in wireless communication technology at terahertz frequencies, there is a growing demand for multifunctional devices such as antennas, filters, and absorbers [24]. Research efforts have focused on utilizing graphene in the design of these devices to operate efficiently at terahertz frequencies [25]. Recent studies have explored the characteristics of graphene antennas, tunable absorbers, and various graphene-based devices, including modulators, sensors, attenuators, power dividers, optical splitters, and switches [26-34]. This article introduces a novel plasmonic filtering device that leverages a distinctive geometric arrangement involving a graphene-based rectangular ring resonator featuring dual minimal apertures. The investigation encompasses the examination of transmission spectra and the distribution of electric fields within the filtering apparatus. Employing advanced three-dimensional finite-difference time-domain (FDTD) simulations with perfect matching layer (PML) absorbing boundary conditions, the study systematically explores the influence of both structural parameters and the chemical potential of graphene on the transmission spectra. Unlike conventional configurations, this innovative design allows for the manipulation of the working frequency range and the transmission peak frequency by dynamically adjusting the width of graphene nanoribbons (GNRs). Furthermore, the bandwidth of the filter is finely tunable through the manipulation of various coupling distances between the lateral waveguide and the rectangular ring resonator. Remarkably, the resonant frequencies exhibit facile control by judiciously altering the chemical potential of graphene. This intrinsic capability enables the realization of an electrically tunable pass-band filter without necessitating modifications to the structural parameters. Notably, the proposed plasmonic filter demonstrates exceptional sensitivity to diverse surrounding mediums, underscoring its potential application as a highly responsive biosensor. Importantly, this groundbreaking structure contributes to the miniaturization of plasmonic filters, opening avenues for their integration into compact plasmonic circuits.

2. Models and discussion

In this description, a portrayal of a suggested filter is presented, constructed based on two graphene rectangular resonators with double narrow gaps. The structure includes incoming and outgoing waveguides as well as a rectangular resonator with two narrow gaps. In this configuration, parameters such as nanoribbon width, resonator width, the length of coupling between the lateral waveguide and the resonator, and gap width are present. The graphene layer is deposited on a substrate with a dielectric constant of ε_r = 1.98. Figure 1 illustrates the schematic diagram of the proposed filter, comprising input and output waveguides along with a rectangular ring resonator featuring double narrow gaps. In this context, a represents the nanoribbon width, b and c stand for the rectangular ring resonator length, l is the width, d denotes the coupling length between the lateral waveguide and the resonator, and g corresponds to the gap width. The suggested filter dimensions are explained in Table 1.

Table 1. Specifications of Graphene Filter with Two Slit Resonators

a (nm)	20
b (nm)	85
c (nm)	45
d (nm)	5
l (nm)	5
g (nm)	10
μ_c (eV)	0.2
substrate	$\varepsilon_r = 1.98$
f (TZ)	2-14

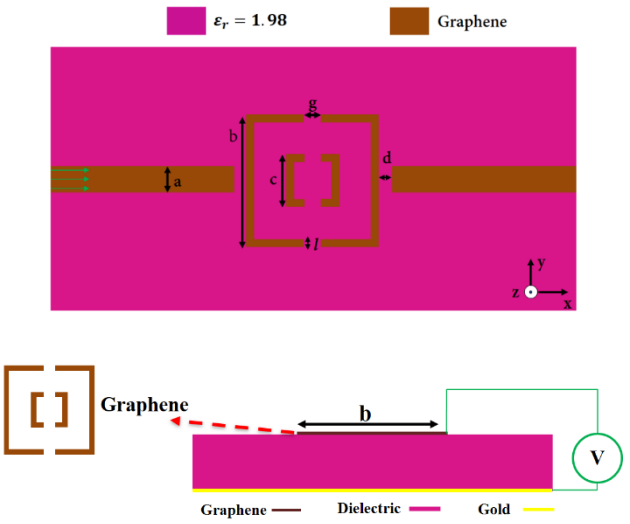

Figure 1. depicts the schematic illustration of the filter utilizing two rectangular ring resonators with dual slits.

Here, a denotes the nanoribbon width, b and c are the length, l is the width of the rectangular resonator, d represents the coupling length between the lateral waveguide and the resonator, and g signifies the gap width. The inset provides a

lateral perspective of the proposed filter featuring a graphene nanoribbon positioned on the substrat. At mid-infrared frequencies, the interband transition is minimized, allowing the use of the simplified Kubo formula for calculating the complex surface conductivity of graphene [35].

$$\sigma_g = \frac{-ie^2 K_B T}{\pi\hbar^2(\omega - i2\Gamma)}\left[\frac{\mu_c}{K_B T} + 2ln\left(e^{-\frac{\mu_c}{K_B T}} + 1\right)\right] \quad (1)$$

where e is the charge of the electron, K_B is Boltzmann's constant, $\hbar$ = h/2π is Planck's constant, ω is the radian frequency, μ_c is the chemical potential, Γ is the scattering rate and T is the temperature. Graphene possesses a fascinating characteristic whereby its chemical potential can be adjusted across a broad spectrum (usually ranging from -1 to 1 eV). This modulation is achieved by the implementation of a transverse electric field through a dc-biased structure [36]. If a DC bias voltage is applied to the graphene layer, it allows for quick control of the chemical potential (μ_c) and consequently enables the control of graphene's electrical properties. An approximate closed-form expression has been proposed for the relationship between μ_c and V_g [37].

$$\mu_c = \hbar v_f \sqrt{\frac{\pi\varepsilon_0\varepsilon_r V_g}{e t_{sub}}} \quad (2)$$

The symbols ε_r and ε_0 in the equation represent the permittivity of the substrate and vacuum, respectively. The variable V_g represents the applied bias voltage, while e and v_f correspond to the electron charge and the Fermi velocity (1.1×10^6 m/s in graphene), respectively. On the whole, as the bias voltage (V_g) increases, the chemical potential (μ_c) increases. This implies an increase in the number of holes (in p-type) or electrons (in n-type) in the graphene layer. These changes in the carrier concentration can induce variations in the conductivity and electronic properties of graphene. The FDTD method with PML absorbing boundary conditions is employed to explore the transmission properties of the structure. Two power monitors are positioned at Port in and Port out to measure the input power (P_{in}) and the transmitted power (P_{out}). Therefore, the transmissivity can be calculated as:

$$T = P_{out}/P_{in} \quad (3)$$

First, we examine a regular rectangular ring resonator filter without gaps [38]. Subsequently, we design a graphene-based slotted rectangular ring filter [32] and place a source on the left side to excite the fundamental edge mode in graphene nanoribbons. Then, the GSP (Graphene Surface Plasmon) edge mode will be coupled into the rectangular ring resonator. Eventually, the GSP wave, meeting specific resonance criteria, can be efficiently coupled to the output port.

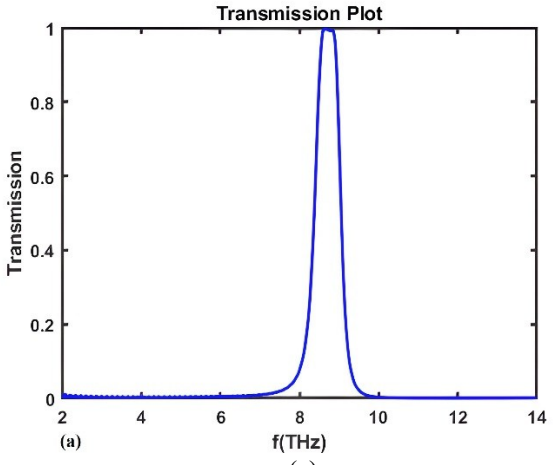

(a)

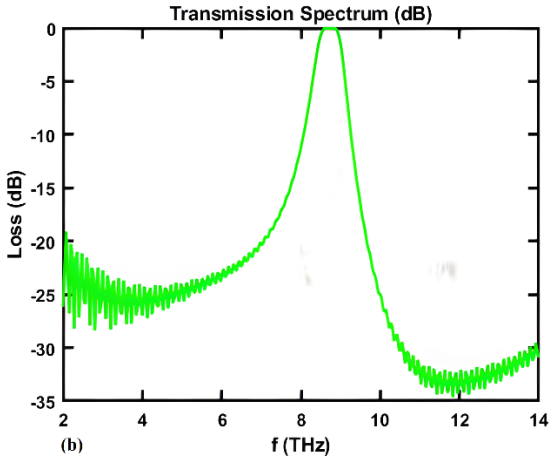

(b)

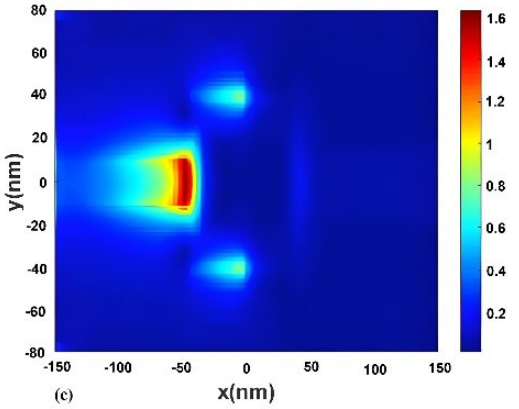

(c)

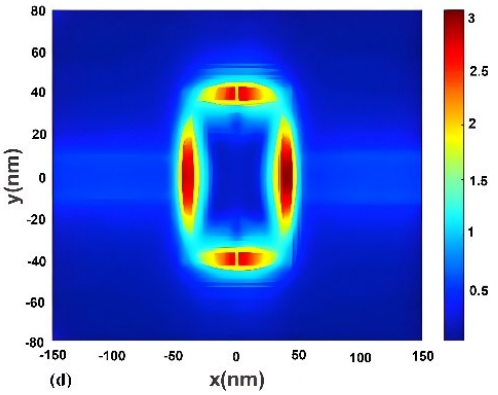

(d)

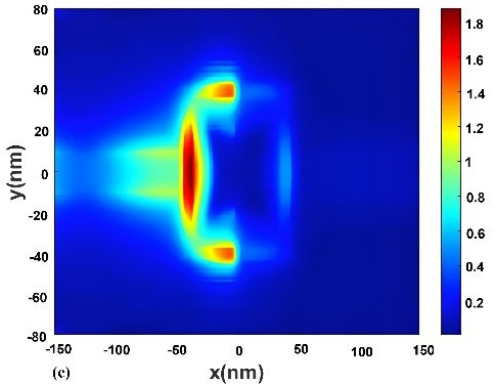

(d)

Figure 2. (a) Filter Transfer Diagram, (b) Filter Loss Diagram, (c) Electric Field Distribution (E_x) in f=7 THz, (d) Electric Field Distribution (E_x) in f=8.66 THz, (e) Electric Field Distribution (E_x) in f=9.5 THz

Figure 2 presents the frequency response of the proposed filter, as described in Table 1. Figure 2a illustrates a unique mode response at a frequency of 8.66 terahertz, with a magnitude of 0.99, showcasing the exceptional performance and efficiency of the filter. The filter's effectiveness in eliminating unwanted frequencies is underscored by the loss graph shown in Figure 2b. Figure 2c showcases the distribution of the electric field (Ex) across frequencies of 7, 8.66, and 9.5 terahertz. Notably, at the resonant frequency of 8.66 THz, the filter rings exhibit the highest level of electric field.

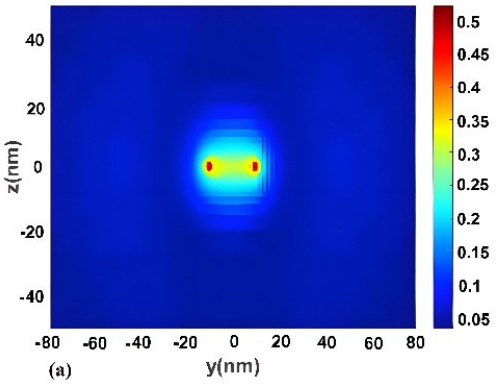

(a)

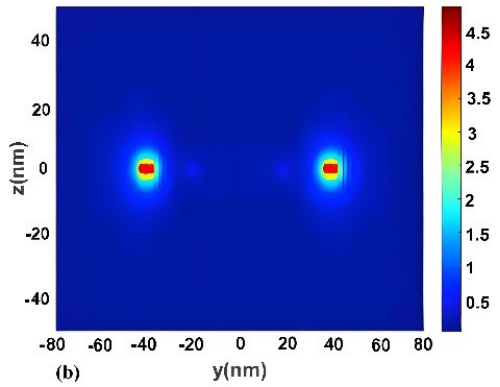

(b)

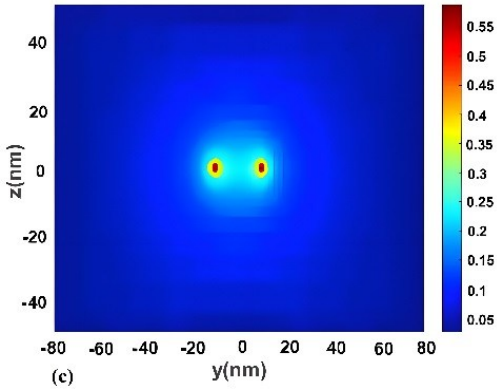

(c)

Figure 3. Electric Field Distribution (E_z) in f=8.66 THz (a) Input (b) Center of rings (c) Output

Based on the propagation characteristics of the wave in the transverse cross-section of the proposed filter, which illustrates the distribution of the electric field E_z at a frequency of 8.66 terahertz at three points: input, output, and center of the square loops, it can be observed that at this frequency, nearly the entire input electric field is present at the output of the filter. (Figure 3)

3. Results and Descriptions

Based on the observed results in Figure 2(a), the proposed filter demonstrates a unique transmission mode with the maximum output magnitude. To explore the potential of the filter further, the dimensions of the filter structure were varied by manipulating different parameters. The obtained results were then compared to evaluate the effects of these changes. In the initial phase, the widths of the input and output ports were varied from 16 nanometers to 24 nanometers. The results of this variation in the filter's performance can be observed in Figure 4. The best output is achieved when a=20 nm.

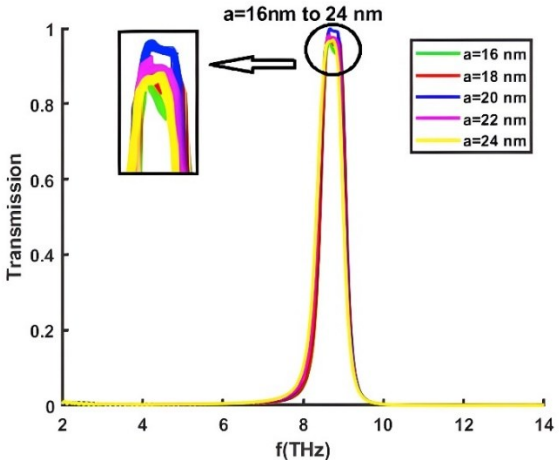

Figure 4. illustrates the impact of varying the input and output port widths on the filter's transfer function.

In the next step, we changed the width of the inner and outer square loops from 4 nanometers to 7 nanometers, as shown in Figure 5. The best filter response in the time domain occurs when the value of l is 5 nm.

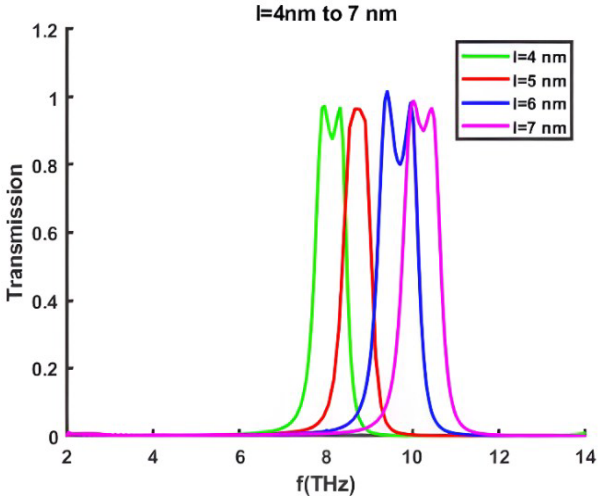

Figure 5. illustrates the effect of changing the width of the inner and outer square loops on the filter transfer plot.

After determining the optimal dimensions of the rings and input/output ports, it is necessary to find suitable gap distances that would yield the best results in the output of the designed filter. To achieve this, we initially consider the rings without any gaps (g=0), and then we gradually introduce gap distances of 5, 10, and 15 nanometers between the rings, respectively (see Figure 6).

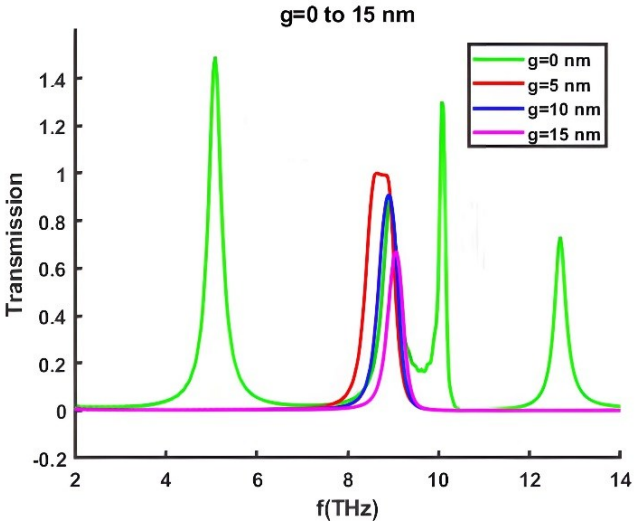

Figure 6. The effect of the gap between loops on the filter transfer function graph.

In the configuration depicted in Figure 6, when the loops are devoid of gaps, the filter exhibits multimodal behavior. The optimum performance of the filter occurs when there is an air gap distance of precisely 5 nanometers.

In the following step, the impact of the spacing between input and output ports on the performance of the proposed filter was examined (Figure 7). Initially, the input and output ports were connected to the first loop (d=0), and subsequently, the spacing between the input and output ports was varied to 3, 5, and 8 nanometers, respectively. According to Figure 7, the optimal performance of the filter was observed when the value of dd was set to 5 nm.

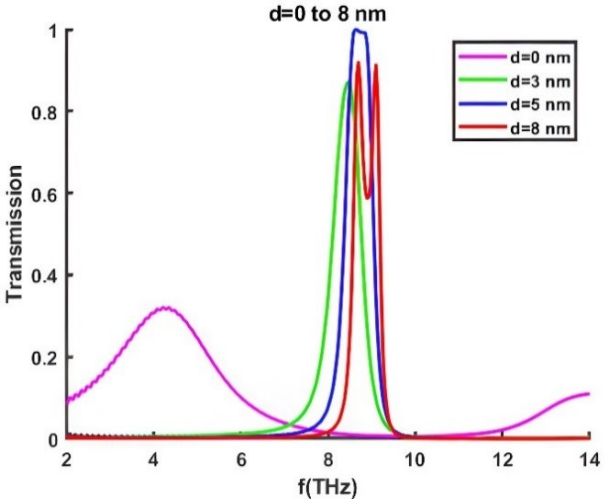

.

Figure 7. Effect of changing the distance between the input and output ports on the proposed filter structure's performance.

After optimizing the dimensions of the structure, we now investigate the frequency response of the graphene bias voltage ranging from 0.18 to 0.4 electron volts. The results of this analysis can be observed in Figure 8.

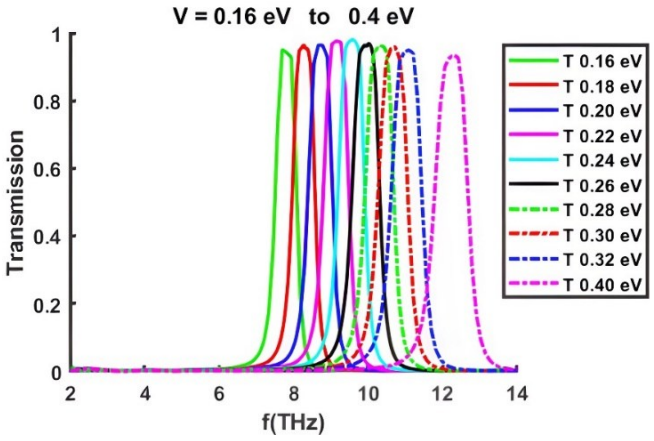

Figure 8. shows the effect of changing the graphene bias voltage from 0.18 to 0.4 electron volts on the transfer characteristic of the filter.

As seen in Figure 5, changing the graphene voltage alters the operating frequency of the filter from 8.2 terahertz to 12.2 terahertz. In various proposed structures for graphene filters, adjusting the graphene bias voltage not only changes the

operating frequency of the structure but also significantly affects the passband range of the filter, potentially leading to a drastic decrease in filter efficiency. However, frequency response analysis of such filters, compared to similar graphene filters, indicates that changing the graphene bias voltage does not cause significant variations in the passband range of the filter, and the filter operates effectively within the studied frequency range. A comparative analysis of different types of graphene filters published in previous articles is presented in Table 2. Compared to different structures, the proposed structure not only has the smallest dimensions and is single-mode, but it also exhibits the best frequency response.

4. Conclusion

In this article, a plasmonic filter based on two rectangular slotted graphene rings is presented. The simulation results using the FDTD method demonstrate that the transmission spectrum of the filter can be influenced by the width of the graphene nanowire, the bandwidth of the input and output ports, and the chemical potential of graphene. One advantage of this structure is its single-mode nature in the proposed frequency band, as well as the unchanged range of the filter transmission curve with variations in the chemical potential. Considering these advantages and the small dimensions of this structure, it finds attractive applications in integrated photonic circuits and optical sensors.

References

[1] Chen, H., Ma, W., Huang, Z., Zhang, Y., Huang, Y., & Chen, Y. (2019). Graphene-based materials toward microwave and terahertz absorbing stealth technologies. Advanced Optical Materials, 7(8), 1801318.

[2] He, Y., Chen, Y., Zhang, L., Wong, S. W., & Chen, Z. N. (2020). An overview of terahertz antennas. China Communications, 17(7), 124-165.

[3] Akyildiz, I. F., Kak, A., & Nie, S. (2020). 6G and beyond: The future of wireless communications systems. IEEE Access, 8, 133995-134030.

[4] Tataria, H., Shafi, M., Molisch, A. F., Dohler, M., Sjöland, H., & Tufvesson, F. (2020). 6G wireless systems: Vision, requirements, challenges, insights, and opportunities. arXiv preprint arXiv:2008.03213.

[۵] محمدباقر حیدری؛ علی عبدالهی (۲۰۲۴). کوپلرهای گرافنی پلاسمونی برای کاربردهای جاذب راداری. *فصلنامه علمی پژوهش‌های نوین در سامانه‌های دفاع الکترونیکی*، دوره ۳، شماره ۸، صص ۴۰-۳۳.

[٦] ابراهیم چگینی؛ یعقوب خراسانی (۲۰۲۴). گرافن آلایش شده با آلومینیوم برای حسگری گازهای سمی No2 و H2S شبیه‌سازی بر مبنای نظریه تابعی چگالی الکترون. *فصلنامه علمی پژوهش‌های نوین در سامانه‌های دفاع الکترونیکی*، دوره ۳، شماره ۷، صص ۱۷-۱۰.

[7] Han, C., Qu, F., Wang, X., Zhai, X., Li, J., Yu, K., & Zhao, Y. (2024). Terahertz spectroscopy and imaging techniques for herbal medicinal plants detection: a comprehensive review. Critical Reviews in Analytical Chemistry, 54(7), 2485-2499.

[8] Anitha, V., Beohar, A., & Nella, A. (2023). THz imaging technology trends and wide variety of applications: a detailed survey. Plasmonics, 18(2), 441-483.

[9] Mohanty, M., Rath, P. S., Mohapatra, A. G., Mohanty, A., & Nayak, S. (2024). Terahertz waves in biomedicine: Pioneering imaging and sensing for healthcare revolution. In Next Generation Wireless Communication: Advances in Optical, mm-Wave, and THz Technologies (pp. 341-360). Cham: Springer Nature Switzerland.

[10] Mohanta, Y. K., Yugal/Biswas Kishore Mohanta (Kuna), & Mahanta, S. (2024). Graphene-based nanomaterials. IEEE Trans. Terahertz Sci. Technol, 14(5).

Table 2. Illustrates the comparison between parameters and results of several graphene filters.

REF	Year	Filter type	Structure	Dimensions (nm2)	Frequency (THz)	$f_{r\,max}$	Chemical potential (eV)	T max	Number of modes
[32]	2017	Bandpass	Graphene ring resonator	120*120	5-25	25	0.4	0.97	2
[38]	2011	Bandpass	Plasmonic hollow core ring resonator	200*200	150-600	550	-	0.52	2
[39]	2016	Bandpass	Plasmonic split ring graphene	200*200	11-30	13	0.24	0.7	4
[40]	2023	Band stop	Graphene hook-shaped resonator	350*500	2-20	4	0.3	0.9	2
[41]	2018	Band stop	Graphene square ring splitting	100*130	7-19	9.65	0.15	0.6	2
[42]	2019	Band stop	Single-layer graphene sheet	9900*4900	6-15	12.2	0.1-1	0.9	1
This paper	2024	Bandpass	Dual graphene ring resonator	85*85	2-14	8.6	0.2-0.4	0.99	1

[11] Hamza, E. K., & Jaafar, S. N. (2022). Nanotechnology application for wireless communication system. In Nanotechnology for electronic applications (pp. 115-130). Singapore: Springer Nature Singapore.

[12] Blessy, J. J., Jaison, B., & Nareshkumar, M. D. (2024, August). Nano Functionalized Antenna Based IoT Enabled Devices for Health Care Applications. In 2024 First International Conference on Electronics, Communication and Signal Processing (ICECSP) (pp. 1-6). IEEE.

[13] Ram, G. C., Sambaiah, P., Yuvaraj, S., & Kartikeyan, M. V. (2023). Graphene-based filter design using triangular patch resonator for THz applications. Nano Communication Networks, 38, 100477.

[14] Maier, S. A., & Maier, S. A. (2007). Surface plasmon polaritons at metal/insulator interfaces. Plasmonics: Fundamentals and Applications, 21-37.

[15] Lee, S. A., & Link, S. (2021). Chemical interface damping of surface plasmon resonances. Accounts of Chemical Research, 54(8), 1950-1960.

[16] Zhang, J., Zhang, L., & Xu, W. (2012). Surface plasmon polaritons: physics and applications. Journal of Physics D: Applied Physics, 45(11), 113001.

[17] Fang, Y., & Sun, M. (2015). Nanoplasmonic waveguides: towards applications in integrated nanophotonic circuits. Light: Science & Applications, 4(6), e294-e294.

[18] Wang, C., Murugadoss, V., Kong, J., He, Z., Mai, X., Shao, Q., ... & Guo, Z. (2018). Overview of carbon nanostructures and nanocomposites for electromagnetic wave shielding. Carbon, 140, 696-733.

[19] Jun, S. C. (2015). Fundamental of graphene. Graphene-based Energy Devices, 1-48.

[20] Otsuji, T., Popov, V., & Ryzhii, V. (2014). Active graphene plasmonics for terahertz device applications. Journal of Physics D: Applied Physics, 47(9), 094006.

[21] Low, T., & Avouris, P. (2014). Graphene plasmonics for terahertz to mid-infrared applications. ACS nano, 8(2), 1086-1101.

[22] Correas-Serrano, D., Gomez-Diaz, J. S., Perruisseau-Carrier, J., & Alvarez-Melcon, A. (2014). Graphene-based plasmonic tunable low-pass filters in the terahertz band. IEEE Transactions on Nanotechnology, 13(6), 1145-1153.

[23] Deng, Y., Cao, G., Yang, H., Zhou, X., & Wu, Y. (2018). Dynamic control of double plasmon-induced transparencies in aperture-coupled waveguide-cavity system. Plasmonics, 13, 345-352.

[24] Chen, Z., Ma, X., Zhang, B., Zhang, Y., Niu, Z., Kuang, N., ... & Li, S. (2019). A survey on terahertz communications. China Communications, 16(2), 1-35.

[25] Chen, H., Ma, W., Huang, Z., Zhang, Y., Huang, Y., & Chen, Y. (2019). Graphene-based materials toward microwave and terahertz absorbing stealth technologies. Advanced Optical Materials, 7(8), 1801318.

[26] Huo, K. L., Yang, S. H., Zong, J. Y., Chu, J. J., Wang, Y. D., & Cao, M. S. (2023). Carbon-based EM functional materials and multi-band microwave devices: Current progress and perspectives. Carbon, 118193.

[27] Wang, L., An, N., He, X., Zhang, X., Zhu, A., Yao, B., & Zhang, Y. (2022). Dynamic and active THz graphene metamaterial devices. Nanomaterials, 12(12), 2097.

[28] Talati, Saeed, Seyed Morteza Ghazali, and VahidReza SoltaniNia. "Design and construct full invisible band metamaterial-based coating with layer-by-layer structure in the microwave range from 8 to 10 GHz." Journal of Physics D: Applied Physics 56.17 (2023): 175401

[29] Cao, G., Li, H., Deng, Y., Zhan, S., He, Z., & Li, B. (2014). Systematic theoretical analysis of selective-mode plasmonic filter based on aperture-side-coupled slot cavity. Plasmonics, 9, 1163-1169.

[30] Barnes, W. L., Dereux, A., & Ebbesen, T. W. (2003). Surface plasmon subwavelength optics. nature, 424(6950), 824-830.

[31] Su, W. (2018). A four-port ultra-compact terahertz splitting filter based on graphene nanoribbon. IEEE Photonics Technology Letters, 31(1), 86-89.

[32] Su, W., & Chen, B. (2017). Graphene-based tunable terahertz filter with rectangular ring resonator containing double narrow gaps. Pramana, 89, 1-5.

[33] Cai, Y., Da Xu, K., Guo, R., Zhu, J., & Liu, Q. H. (2018). Graphene-based plasmonic tunable dual-band bandstop filter in the far-infrared region. IEEE Photonics Journal, 10(6), 1-9.

[34] Sensale-Rodriguez, B., Yan, R., Zhu, M., Jena, D., Liu, L., & Grace Xing, H. (2012). Efficient terahertz electro-absorption modulation employing graphene plasmonic structures. Applied Physics Letters, 101(26).

[35] Hanson, G. W. (2008). Dyadic Green's functions and guided surface waves for a surface conductivity model of graphene. Journal of Applied Physics, 103(6).

[36] Correas-Serrano, D., Gomez-Diaz, J. S., Perruisseau-Carrier, J., & Alvarez-Melcon, A. (2014). Graphene-based plasmonic tunable low-pass filters in the terahertz band. IEEE Transactions on Nanotechnology, 13(6), 1145-1153.

[37] Gómez-Díaz, J. S., & Perruisseau-Carrier, J. (2013). Graphene-based plasmonic switches at near-infrared frequencies. Optics Express, 21(13), 15490-15504.

[38] Setayesh, A., Mirnaziry, S. R., & Abrishamian, M. S. (2011). Numerical investigation of a tunable band-pass plasmonic filter with a hollow-core ring resonator. Journal of Optics, 13(3), 035004.

[39] Gao, Y., Ren, G., Zhu, B., Huang, L., Li, H., Yin, B., & Jian, S. (2016). Tunable plasmonic filter based on graphene split-ring. Plasmonics, 11, 291-296.

[40] Zonouri, S. A., & Hayati, M. (2023). A compact graphene-based dual-band band-stop filter using new hook-shaped resonator for THz applications. Materials Science in Semiconductor Processing, 153, 107150.

[41] Zhuang, H., Xu, H., Kong, F., Wang, Y., Gao, M., & Li, K. (2018). Tunable slow light based on detuned coupling between graphene nanoribbon and square ring splitting modes. Optical and Quantum Electronics, 50, 1-10.

[42] Abbas, M. N., & Khaleel, F. A. (2019). Wide-range tunable subwavelength band-stop filter for the far-infrared wavelengths based on single-layer graphene sheet. Ukrainian journal of physical optics, (20, № 1), 37-45.